Direct Numerical Simulation of Turbulence/Radiation Interaction in Premixed Combustion Systems

Y. Wu [a] D.C. Haworth* [a] M.F. Modest [a] B. Cuenot [b]

[a] *Department of Mechanical & Nuclear Engineering, The Pennsylvania State University, University Park, PA, USA*

[b] *Centre Européen de Recherche et de Formation Avancée en Calcul Scientifique, Toulouse, France*

*Corresponding Author:
232 Research Building East
University Park, PA 16802 USA
Voice: 814 863-6269 Fax: 814 865-3389 Email: dch12@psu.edu

Colloquium 5: Turbulent Flames

Running title: *DNS of Turbulence/Radiation Interaction*

Total length: 5980 words
Main text: 4140 words (word count utility)
Equations: 290 words (38 lines × 7.6 words/line)
References: 420 words (22 references; 24 × 2.3 × 7.6)
Table 1: 110 words (15 lines × 7.6 words/line)
Figure 1: 320 words (double column, $h/w = 0.4$, 45-word caption)
Figure 2: 160 words (single column, $h/w = 0.7$, 40-word caption)
Figure 3: 270 words (double column, $h/w = 0.35$, 25-word caption)
Figure 4: 270 words (double column, $h/w = 0.35$, 25-word caption)

Abstract

An important fundamental issue in chemically reacting turbulent flows is turbulence/radiation interaction (TRI); TRI arises from highly nonlinear coupling between temperature and composition fluctuations. Here a photon Monte Carlo method for the solution of the radiative transfer equation (RTE) has been integrated into a turbulent combustion direct numerical simulation (DNS) code. DNS then has been used to investigate TRI in a canonical configuration with systematic variations in optical thickness. The formulation allows for nongray gas properties, scattering, and general boundary treatments, although in this study, attention has been limited to gray radiation properties, no scattering, and black boundaries. Individual contributions to emission and absorption TRI have been isolated and quantified. Of particular interest are intermediate values of optical thickness where, for example, the smallest hydrodynamic and chemical scales are optically thin while the largest turbulence scales approach optically thick behavior. In the configuration investigated, the temperature self-correlation contribution (emission) is primarily a function of the ratio of burned-gas temperature to unburned-gas temperature, and is the dominant contribution to TRI only in the optically thin limit. Even in the most optically thin case considered, the absorption coefficient-Planck function correlation and absorption coefficient-intensity correlation are not negligible. At intermediate values of optical thickness, contributions from all three correlations are significant.

Key words: Turbulence/radiation interaction, Direct numerical simulation, Photon Monte Carlo method

1 Introduction

Thermal radiation often is a dominant mode of heat transfer in practical turbulent combustion systems. By contrast to conduction and convection, consideration of thermal radiation leads to an integral equation in up to six independent variables; radiative heat transfer rates vary strongly with temperature differences (to the fourth or higher power); and the radiation properties of combustion gases exhibit strong and irregular variations with wavenumber [1]. For these reasons and others, radiation often has been neglected altogether or has been treated using simple models (e.g., an optically thin approximation) in combustion applications.

The importance of interactions between turbulence and thermal radiation (turbulence/radiation interaction – TRI) has long been recognized [2–6]. TRI arises from highly nonlinear coupling between temperature and composition fluctuations in both nonreacting and reacting turbulent flows. In this respect, TRI is akin to the turbulence/chemistry interaction [7] that has been the subject of intense research for many years. TRI has been shown to result in significant increases in overall heat transfer, significant reductions in local temperature, and consequently in significant changes in key pollutant species (particularly NOx and soot) in both luminous and nonluminous turbulent flames (e.g., [4,6,8–13]). TRI effects can be comparable to those resulting from turbulence/chemistry interaction. Yet TRI modeling has received relatively little attention to date.

Direct numerical simulation (DNS) has become an accepted tool for generating new fundamental insight into turbulence/chemistry interaction (e.g., [14,15]). Here DNS is used to explore turbulence/radiation interaction in idealized systems. The goals are to develop new fundamental physical insight and to provide guidance for model

development. The nature of turbulence/radiation interaction is discussed in Section 2. The model problem is outlined in Section 3. Numerical methods are described briefly in Section 4, and results and discussion are provided in Section 5. Conclusions and next steps are summarized in the final section.

2 Turbulence/Radiation Interaction in Chemically Reacting Flows

The radiation source term in the instantaneous energy equation can be expressed as the divergence of the radiative heat flux $\vec{q}_{rad}$,

$$\nabla \cdot \vec{q}_{rad} = \int_0^\infty \kappa_\eta \Big(4\pi I_{b\eta} - \int_{4\pi} I_\eta d\Omega \Big) d\eta = 4\kappa_P \sigma T^4 - \int_0^\infty \int_{4\pi} \kappa_\eta I_\eta d\Omega d\eta \ , \qquad (1)$$

where

$$\kappa_P \equiv \frac{\int_0^\infty \kappa_\eta I_{b\eta} d\eta}{\int_0^\infty I_{b\eta} d\eta} = \frac{\pi}{\sigma T^4} \int_0^\infty \kappa_\eta I_{b\eta} d\eta \qquad (2)$$

is the Planck-mean absorption coefficient and σ is the Stefan-Boltzmann constant. Here η denotes wavenumber, Ω is solid angle, κ_η is the spectral absorption coefficient, $I_{b\eta}$ is the Planck function (a known function of local temperature and wavenumber), and I_η is the spectral radiative intensity. Intensity is determined from the radiative transfer equation (RTE) [1]:

$$\frac{dI_\eta}{ds} = \hat{s} \cdot \nabla I_\eta = \kappa_\eta I_{b\eta} - \beta_\eta I_\eta + \frac{\sigma_{s\eta}}{4\pi} \int_{4\pi} I_\eta(\hat{s}_i) \Phi_\eta(\hat{s}_i, \hat{s}) d\Omega_i \ . \qquad (3)$$

Here $\hat{s}$ and $\hat{s}_i$ denote unit direction vectors, $\sigma_{s\eta}$ is the spectral scattering coefficient, $\beta_\eta = \kappa_\eta + \sigma_{s\eta}$ is the spectral extinction coefficient, and $\Phi_\eta(\hat{s}_i, \hat{s})$ denotes the scattering phase function; the latter describes the probability that a ray from incident direction $\hat{s}_i$ is scattered into direction $\hat{s}$. The local value of I_η depends on nonlocal quantities, on direction ($\hat{s}$), and on wavenumber.

The first term on the right-hand side of Eq. (1) corresponds to emission and the

second to absorption. TRI is brought into evidence by taking the mean of Eq. (1):

$$\langle \nabla \cdot \vec{q}_{rad} \rangle = \int_0^\infty \left(4\pi \langle \kappa_\eta I_{b\eta} \rangle - \int_{4\pi} \langle \kappa_\eta I_\eta \rangle d\Omega \right) d\eta = 4\sigma \langle \kappa_P T^4 \rangle - \int_0^\infty \langle \kappa_\eta G_\eta \rangle d\eta \ , \quad (4)$$

where angled brackets denote mean quantities, and the direction-integrated incident radiation $G_\eta \equiv \int_{4\pi} I_\eta d\Omega$ has been introduced.

In the emission term, TRI appears as a correlation between the spectral absorption coefficient and the Planck function or, equivalently, between the Planck-mean absorption coefficient and the fourth power of temperature: $\langle \kappa_P T^4 \rangle = \langle \kappa_P \rangle \langle T^4 \rangle + \langle \kappa_P' \cdot (T^4)' \rangle$, where a prime denotes a fluctuation about the local mean. Emission TRI can be decomposed to consider separately the temperature self-correlation ($\langle T^4 \rangle \neq \langle T \rangle^4$) and the absorption coefficient-Planck function correlation. Radiative emission including TRI appears in closed form in one-point probability density function (PDF) approaches [11,12]. Li and Modest [12] used a PDF method to examine individual contributions of various correlations to TRI in turbulent nonpremixed flames.

In the absorption term, TRI appears as a correlation between the spectral absorption coefficient and the spectral intensity (or incident radiation), $\langle \kappa_\eta G_\eta \rangle = \langle \kappa_\eta \rangle \langle G_\eta \rangle + \langle \kappa_\eta' G_\eta' \rangle$. A dimensionless optical thickness is introduced, $\kappa_\eta L$, where L is a length scale. In the "optically thin eddy" approximation ($\kappa_\eta L \ll 1$), fluctuations in κ_η (a local quantity) are assumed to be uncorrelated with those in G_η (a nonlocal quantity), so that $\langle \kappa_\eta G_\eta \rangle \approx \langle \kappa_\eta \rangle \langle G_\eta \rangle$. At the other extreme ($\kappa_\eta L \gg 1$), the optical thickness may be large compared to *all* hydrodynamic and chemical scales. In that case, fluctuations in intensity are generated locally and would be expected to be correlated strongly with those of the absorption coefficient. Between these extremes are cases where the smallest scales (Kolmogorov microscales and/or flame thickness) are optically thin while the largest (integral scales) are optically thick. The physics and modeling of "optically thick eddies" is an outstanding issue in TRI, and is a primary motivation

for this research.

Experimental measurements (e.g., [8,9]), theoretical analysis (e.g., [10]), and computational studies (e.g., [4,11,12]) have quantified the importance of TRI in several turbulent reacting flows. It has been shown that radiative emission from a flame can be 50% to 200% higher than would be expected based on mean values of temperature and absorption coefficient, and that local gas temperatures can be reduced by as much as 200°C with TRI compared to radiation heat transfer without TRI. These effects are important for nonsooting flames as well as for highly sooting flames.

In the present study, we explore TRI in a statistically one-dimensional turbulent premixed system using DNS. The principal quantities examined are the normalized means $\mathcal{R}_{T^4}$, $\mathcal{R}_{\kappa I_b}$, and $\mathcal{R}_{\kappa G}$,

$$\mathcal{R}_{T^4} \equiv \frac{\langle T^4 \rangle}{\langle T \rangle^4} \ , \ \mathcal{R}_{\kappa I_b} \equiv \frac{\langle \kappa_\eta I_{b\eta} \rangle}{\langle \kappa_\eta \rangle \langle I_{b\eta} \rangle} \ , \ \mathcal{R}_{\kappa G} \equiv \frac{\langle \kappa_\eta G_\eta \rangle}{\langle \kappa_\eta \rangle \langle G_\eta \rangle} \ , \tag{5}$$

and the correlation coefficients $\rho_{\kappa I_b}$ and $\rho_{\kappa G}$,

$$\rho_{\kappa I_b} \equiv \frac{\langle \kappa'_\eta I'_{b\eta} \rangle}{[\langle \kappa'^2_\eta \rangle \langle I'^2_{b\eta} \rangle]^{1/2}} \ , \ \rho_{\kappa G} \equiv \frac{\langle \kappa'_\eta G'_\eta \rangle}{[\langle \kappa'^2_\eta \rangle \langle G'^2_\eta \rangle]^{1/2}} \ . \tag{6}$$

In the absence of TRI, $\mathcal{R}_{T^4}$, $\mathcal{R}_{\kappa I_b}$, and $\mathcal{R}_{\kappa G}$ would be equal to unity while $\rho_{\kappa G}$ would be equal to zero. The departures of each quantity from these values allow different contributions to TRI to be isolated and quantified.

3 Physical Models and Computational Configuration

A turbulent, compressible, chemically reacting, radiatively participating ideal-gas mixture is considered. The continuity, linear momentum, chemical species, and energy equations have the same form as in [14], with the addition of a thermal radiation

source term in the energy equation. Thus,

$$\frac{\partial \rho e_t}{\partial t} + \nabla \cdot (\rho e_t + p)\vec{u} = \frac{\partial (u_i \tau_{ij})}{\partial x_j} + \nabla \cdot (\lambda \nabla T) + Q\dot{w} - \nabla \cdot \vec{q}_{rad} \ . \tag{7}$$

Here $\vec{u}$ is the fluid velocity vector, ρ is the fluid mass density, p is the thermodynamic pressure, τ_{ij} are the components of the viscous stress tensor, Q is the heat of reaction per unit mass of fresh mixture, and ρe_t is the total energy density per unit volume, $\rho e_t \equiv \rho \vec{u} \cdot \vec{u}/2 + p/(\gamma - 1)$, where γ is the (constant) ratio of specific heats.

Single-step irreversible finite-rate Arrhenius chemistry is considered. The reaction rate is $\dot{w} = \mathcal{B}\rho \tilde{Y}_R \exp\Big\{-\beta(1-\Theta)/[1-\alpha(1-\Theta)]\Big\}$, where Θ is the reduced temperature, $\Theta = (T - T_1)/(T_2 - T_1)$, and subscript '1' refers to the fresh gases and '2' to the burned products (T_2 is the constant-pressure adiabatic flame temperature). The coefficients $\mathcal{B}$, α, and β are, respectively, the reduced pre-exponential factor, the temperature factor, and the reduced activation energy, and $\tilde{Y}_R$ is a normalized reactant mass fraction that varies from unity in the fresh gases to zero in the burned gases. Standard molecular transport models (Newtonian viscosity, Fourier conduction, and Fickian species diffusion) are employed where the molecular transport coefficients (viscosity μ, thermal conductivity λ, and species diffusion coefficient $\mathcal{D}$) are set such that the Prandtl number Pr and Lewis number Le are constant. Soret and Dufour effects are not included.

Here the divergence of the radiation heat flux is determined by solving the RTE, Eq. (3), using a photon Monte Carlo method (Section 4). Radiation properties correspond to a fictitious gray gas with Planck-mean absorption coefficient,

$$\begin{aligned} \kappa_p = & C_\kappa (Y_P + \epsilon_Y) \times \\ & \left[c_0 + c_1 \left(\frac{A}{T}\right) + c_2 \left(\frac{A}{T}\right)^2 + c_3 \left(\frac{A}{T}\right)^3 + c_4 \left(\frac{A}{T}\right)^4 + c_5 \left(\frac{A}{T}\right)^5 \right] , \end{aligned} \tag{8}$$

where $Y_P \equiv 1 - \tilde{Y}_R$ is a normalized reaction progress variable. Coefficients A and

c_0–c_5 have been taken from a radiation model suggested for water vapor [16], with the temperature rescaled to the computational temperature range. Here ϵ_Y is an arbitrary, small, positive threshold to ensure that κ_P is nonzero everywhere, and C_κ is a coefficient that allows the optical thickness to be varied systematically and independently of other parameters. For fixed values of C_κ and Y_P, κ_P varies by more than a factor of ten over the temperature range of interest.

The governing equations are solved for a statistically one-dimensional turbulent premixed system. The configuration is periodic in the y- and z-directions, and $-x$ is the direction of (mean) flame propagation (Fig. 1). An initial turbulence spectrum is prescribed using methods that have been developed for earlier DNS studies [14,17]. A one-dimensional premixed laminar flame profile is superposed on the initial turbulence field, and the system is allowed to evolve in time. Key parameters are the thermochemical quantities ($\mathcal{B}$, α, β, Pr, Le, γ, κ_P), the initial turbulence integral length scale l_0 (the two-point longitudinal integral length scale, l_{11}, or the wavelength of the most energetic eddies in the initial turbulence spectrum, L_i [14]) and rms turbulence level u'_0, and the undisturbed steady one-dimensional laminar flame speed s_l and flame thickness δ_l. Key dimensionless parameters are a turbulence Reynolds number $Re_0 \equiv \rho_1 u'_0 l_{11}/\mu_1$, the ratios u'_0/s_l and L_i/δ_l, and a Damköhler number $Da \equiv \mathcal{B}\mathcal{D}/s_l^2 \exp(-\beta/\alpha)$. The values specified for these quantities are similar to those used in [14] (Table 1). A new dimensionless parameter is introduced to characterize thermal radiation: $\kappa_{P,2} l_{11}$, the optical thickness based on burned-gas properties and the initial turbulence integral length scale.

As the system evolves, u' decays while l increases such that the turbulence Reynolds number $\rho_1 u' l/\mu_1$ increases with time. From earlier studies [14], it is known that flame statistics become approximately stationary after two to three eddy-turnover times. Here the system is allowed to evolve for three eddy-turnover times before the radiation

model is activated. The system then evolves for one additional turnover time. Mean quantities are estimated by averaging over the y- and z-directions; these then are displayed as functions of $\langle Y_P \rangle$ through the turbulent flame brush.

The present study follows earlier DNS work for turbulence/chemistry interaction (e.g., [14]) both in spirit and in form. Most of the simulations are spatially two-dimensional. Previous studies have shown relatively small differences between two- and three-dimensional statistics when the focus is on flame/turbulence interaction. This issue has been discussed by Haworth and Poinsot [14]. One three-dimensional case is included for comparison (Table 1). The focus is on quantities [Eqs. (5) and (6)] that are expected to depend weakly on the specific configuration (initial and boundary conditions, spatial two-dimensionality). The model problem is designed to allow systematic variation in key dimensionless parameters (e.g., Re_0, Da, $\kappa_{P,2} l_{11}$) and isolation of generic physical effects.

4 Numerical Methods

4.1 DNS of Chemically Reacting Turbulent Flows

Dimensionless forms of the conservation equations are solved. Temporal integration is performed with a Runge-Kutta method of order three; for spatial discretization, a compact scheme of order six is used in the interior of the computational domain with various noncentered schemes near boundaries [18]. Nonperiodic boundary conditions are enforced using the Navier-Stokes Characteristics Boundary Conditions method [19]. Details of the equations, normalizations, and numerical methods (in the absence of thermal radiation) can be found in Ref. [17].

4.2 A Photon Monte Carlo Method for the Solution of the RTE

The RTE is solved by following the trajectories of a large number of representative photon bundles generated using statistical sampling techniques. A general formulation has been implemented that allows for nongray gas properties, scattering, and a variety of boundary conditions. In the present study we limit our attention to gray radiation properties, no scattering, and black boundaries. The general spectral formulation is outlined in the following. A photon Monte Carlo method for a participating medium consists of two parts: an emission stage and a tracing/absorption/scattering stage. Additional considerations are required at boundaries of the computational domain. The approach that has been implemented essentially follows the method outlined in Chapter 20 of Modest [1]. High-order schemes having accuracy commensurate with that of the underlying DNS code (up to sixth order in space) have been employed throughout.

4.2.1 Emission

Each photon bundle represents a specified fraction of the total emitted radiant energy, E_V, and is characterized by six quantities: an emission location (three spatial coordinates for volume emission, two for surface emission), an emission direction (azimuth angle ψ, polar angle θ), and a spectral variable (wavenumber η). These properties are determined based on the probabilities of events in the reacting gas mixture. As an example, emission locations are determined as follows. First, the local Planck-mean absorption coefficient κ_P (a function of local temperature, pressure, and composition) is computed at each grid point. The total emission from the gas volume V is then,

$$E_V = \int_V 4\kappa_P \sigma T^4 dV = \int_0^{L_x} \int_0^{L_y} \int_0^{L_z} 4\kappa_P \sigma T^4 dz dy dx \ . \tag{9}$$

The cumulative distribution functions (CDF's) of emission along the x, y, and z directions are determined sequentially as [1],

$$R_x = \frac{\int_0^x \int_0^{L_y} \int_0^{L_z} 4\kappa_P \sigma T^4 dz dy dx}{E_V} \ , R_y = \frac{\int_0^y \int_0^{L_z} 4\kappa_P \sigma T^4 dz dy}{\int_0^{L_y} \int_0^{L_z} 4\kappa_P \sigma T^4 dz dy} \ ,$$
$$R_z = \frac{\int_0^z 4\kappa_P \sigma T^4 dz}{\int_0^{L_z} 4\kappa_P \sigma T^4 dz} \ , \tag{10}$$

so that R_x, R_y, and R_z each lie between zero and unity. Inversion of Eqs. (10) yields the emission position with R_x, R_y, and R_z each sampled independently from a uniform distribution on [0,1]: $x = x(R_x)$, $y = y(R_y, x)$, $z = z(R_z, x, y)$.

The emission wavenumber and propagation direction are determined in a similar manner. Details can be found in Refs. [1,20]. The results for an isotropic emitter are:

$$R_\eta = \frac{\pi}{\kappa_P \sigma T^4} \int_0^\eta \kappa_\eta I_{b\eta} d\eta \ , \ R_\psi = \frac{\psi}{2\pi} \ , \ R_\theta = \frac{1 - \cos\theta}{2} \ , \tag{11}$$

where R_η, R_ψ, and R_θ are the CDF's of emission wavenumber, azimuth angle ψ, and polar angle θ at emission position (x, y, z), respectively.

4.2.2 Tracing, Absorption, and Scattering

The energy of each photon bundle is attenuated by volumetric absorption in the gas and by interaction with surfaces; its direction may change as a result of scattering. An energy-partitioning scheme [1] is employed for absorption, whereby each bundle's energy is attenuated along its trajectory until the energy becomes negligible or the bundle hits a wall; bundles that strike a wall may be partially reflected, partially transmitted, and partially absorbed. The absorbed energy is assigned to computational grid points using high-order interpolation; this provides the radiation source term in the energy equation. On scattering, a new propagation direction is determined from the CDF's of all possible directions; for isotropic scattering, Eqs. (11) can be

used directly.

4.2.3 Boundary Conditions

In this study, three types of boundaries are considered for radiation (Fig. 1): periodic, "cold," and "hot." When a photon bundle reaches a periodic boundary, it re-enters the computational domain through the opposite side with no change in properties. A bundle that arrives at a cold boundary is absorbed; no photon bundles are emitted from a cold boundary. A hot boundary is treated as a black surface: a bundle that arrives at a hot boundary is absorbed. Emission from a hot boundary is also considered using a two-dimensional analog of Eqs. (9)–(11).

4.2.4 Computational Considerations

Numerical evaluation of Eqs. (9)–(11) involves extensive spatial interpolation; and this interpolation dominates the computational effort. The interpolation order is determined locally and adaptively. For example, low-order interpolation suffices in the reactants well ahead of the flame and in the burned gases well behind the flame. Spatial and temporal accuracy, statistical error, parallelism, adaptivity, and other computational aspects are addressed in Ref. [20].

The computational effort increases in proportion to the number of photon bundles and the average distance that a bundle travels before being absorbed. For the cases reported here, radiation requires approximately ten times the CPU time of the underlying simple-chemistry DNS code. While this is significant, it is important to keep in mind the following. First, the photon Monte Carlo method provides an "exact" solution to the RTE that is compatible with the philosophy of DNS. Alternative methods including spherical harmonics and discrete ordinates invoke significant ap-

proximations and are of limited applicability [1]. Second, consideration of more detailed chemistry (e.g., [21]) implies little additional computational effort for radiation, while the CPU time for the underlying hydro-chemical DNS would increase dramatically; chemical kinetics then would dominate the CPU requirements. And third, the implementation is quite general. Nongray radiation properties, scattering, and solid particle (soot) radiation can be included with little additional computational overhead.

5 Results and Discussion

Emission TRI is examined first. The temperature self-correlation factor $\mathcal{R}_{T^4}$ is plotted as a function of normalized mean reaction progress variable $\langle Y_P \rangle$ in Fig. (2). Results for the four two-dimensional cases (Table 1) are essentially the same. Here and in the following, mean profiles for two-dimensional cases have been smoothed slightly to compensate for the limited information in one-dimensional averages. While temperature self-correlation is considered to be a part of TRI, $\mathcal{R}_{T^4}$ does not depend directly on radiation properties in this configuration. In the limit of an infinitesimally thin flame sheet, the probability of encountering burned gases at any x location is $\langle Y_P(x) \rangle$ and the probability of encountering unburned gases is $1 - \langle Y_P(x) \rangle$. In that case, $\langle T^4 \rangle / \langle T \rangle^4$ is given by,

$$\mathcal{R}_{T^4\,\mathrm{sheet}} = \frac{\langle Y_P \rangle (T_2/T_1)^4 + 1 - \langle Y_P \rangle}{[\langle Y_P \rangle (T_2/T_1) + 1 - \langle Y_P \rangle]^4} \ . \tag{12}$$

This quantity has been plotted as a function of temperature ratio T_2/T_1 in Fig. (2). As T_2/T_1 increases from unity, the peak in $\mathcal{R}_{T^4\,\mathrm{sheet}}$ increases and shifts toward the leading edge of the flame (smaller values of $\langle Y_P \rangle$). The simulated flames ($T_2/T_1 = 4$) have nonzero thickness, and therefore lower values of $\mathcal{R}_{T^4}$ compared to those given by Eq. (12). The two-dimensional DNS results lie between the flamesheet results for

$T_2/T_1 = 3$ and $T_2/T_1 = 4$; the three-dimensional DNS results (smaller L_i/δ_l, Table 1) are close to the flamesheet results for $T_2/T_1 = 3$.

The quantities $\mathcal{R}_{\kappa I_b}$ and $\rho_{\kappa I_b}$ are plotted in Fig. (3). For the three two-dimensional cases (Cases 1–3), the values of these normalized quantities are essentially the same for all values of the optical thickness; the small differences are not statistically significant. That is because the values of $\kappa_P = \kappa_P(Y_P, T)$ for these three cases differ simply by a multiplicative constant [C_κ, Eq. (8)]. Larger differences result from changing the functional form of $\kappa_P(Y_P, T)$ (not shown). The peak value of $\mathcal{R}_{\kappa I_b}$ is between 7 and 8, and occurs close to the leading edge of the turbulent flame brush; it then decreases monotonically to unity through the flame. At the leading edge, $\rho_{\kappa I_b}$ jumps to unity for all values of $\kappa_{P,2} l_{11}$ (perfect correlation between κ_P and I_b); the correlation then decreases monotonically through the flame brush. Thus even in the most optically thin case examined, the absorption coefficient-Planck function contribution to TRI is not negligible. Three-dimensional results (Case 4) are qualitatively similar to the two-dimensional results.

Absorption TRI is examined next (Fig. 4). The approximation $\langle \kappa_P G \rangle \approx \langle \kappa_P \rangle \langle G \rangle$ improves with decreasing optical thickness, as expected. However, even in the most optically thin case examined $\mathcal{R}_{\kappa G}$ ranges from 0.8 to 1.1 through the flame brush. The correlation coefficient $\rho_{\kappa G}$ goes to zero in the burned gas and in the unburned gas for all values of $\kappa_{P,2} l_{11}$. The variation of $\rho_{\kappa G}$ through the flame brush is essentially the same for the intermediate and large optical thicknesses; values are systematically lower, but still non-negligible, for the optically most thin case. Three-dimensional results (Case 4) are similar to two-dimensional results (Case 2) for the same dimensionless optical thickness.

6 Conclusion

Direct numerical simulation has been used to explore turbulence/radiation interaction in an idealized premixed system. Three contributions to TRI have been isolated and quantified as a function of optical thickness: temperature self-correlation, absorption coefficient-Planck function correlation, and absorption coefficient-intensity correlation. Key findings are as follows.

- Temperature self-correlation is primarily a function of the temperature ratio in this configuration.
- Temperature self-correlation is the dominant contribution to TRI only for the most optically thin case. Even in that case, the absorption coefficient-Planck function correlation and absorption coefficient-intensity correlation are not negligible.
- At intermediate values of optical thickness, contributions from all three correlations are significant.

The importance of TRI and other radiation phenomena (e.g., nongray effects [22]) is becoming increasingly evident for practical combustion systems. Here a first step has been taken toward systematically isolating and quantifying TRI effects using DNS. As always, one must exercise caution in extrapolating DNS results to practical combustion systems. The model problem is highly idealized; in particular, the dynamic range of length scales is small. DNS will continue to map out the influence of key dimensionless parameters (e.g., Re, Da, κL), to study the influence of the functional form of $\kappa_P(Y_P, T)$, to explore nongray-gas effects and soot radiation, to study alternative configurations (nonpremixed systems, detailed chemistry and transport), and ultimately to assess and calibrate models suitable for engineering applications.

Acknowledgements

This work has been supported by the National Science Foundation under Grant Number CTS-0121573 and by the Air Force under Grant Number F49620-99-1-0290.

References

[1] M.F. Modest, *Radiative Heat Transfer* (Second edition, Academic Press, 2003).

[2] A. Townsend, *J. Fluid Mech.* **3** (1958) 361–375.

[3] T.H. Song, R. Viskanta, *J. Thermoph. Heat Transfer* **3** (1987) 52–62.

[4] A. Soufiani, P. Mignon, J. Taine, *Proc. Ninth Intern'l. Heat Transfer Conference* **6** (1990) 403–408.

[5] R.J. Hall, A. Vranos, *Intern'l. J. Heat Mass Transfer* **37** (1994) 2745.

[6] S.R. Tieszen, *Ann. Rev. Fluid Mech.* **33** (2001) 67–92.

[7] R.W. Bilger, *Prog. Energy Combust. Sci.* **26** (2000) 367–380.

[8] J.P. Gore, G.M. Faeth, *Proc. Combust. Institute* **21** (1986) 1521–1531.

[9] M.E. Kounalakis, J.P. Gore, G.M. Faeth, *Proc. Combust. Institute* **22** (1988) 1281–1290.

[10] G. Cox, *Combust. Sci. Technol.* **17** (1977) 75–78.

[11] S. Mazumder, M.F. Modest, *Intern'l. J. Heat Mass Transfer* **42** (1998) 971–991.

[12] G. Li, M.F. Modest, *J. Quant. Spectroscopy and Radiat. Transfer* **73** (2002) 461–472.

[13] J.-F. Ripoll, *J. Quant. Spectroscopy and Radiat. Transfer* **83** (2004) 493–517.

[14] D.C. Haworth, T.J. Poinsot, *J. Fluid Mech.* **244** (1992) 405–436.

[15] D. Veynante, L. Vervisch, *Prog. Energy Combust. Sci.* **28** (2002) 193–266.

[16] Combustion Research Facility, Sandia National Laboratories, *Intern'l. Workshop on Measurement and Computation of Turbulent Nonpremixed Flames* (http://www.ca.sandia.gov/TNF/radiation.html, 2002).

[17] M. Baum, Etude de l'allumage et de la structure des flames turbulentes, Ph.D. thesis, Ecole Centrale de Paris (1994).

[18] S. Lele, *J. Comput. Phys.* **103** (1992) 16–42.

[19] T. Poinsot, S. Lele, *J. Comput. Phys.* **101** (1992) 104–129.

[20] Y. Wu, M.F. Modest, D.C. Haworth, Development of a photon Monte Carlo method for direct numerical simulation of chemically reacting turbulent flows. In preparation for submittal to *Combust. Theory & Modelling* (2004).

[21] C. Jiménez, B. Cuenot, T. Poinsot, D. Haworth, *Combust. Flame* **128** (2002) 1–21.

[22] L. Wang, D.C. Haworth, S.R. Turns, M.F. Modest, Interactions among soot, thermal radiation, and NOx emissions in oxygen-enriched turbulent nonpremixed flames: a CFD modeling study. Submitted to *30'th Intern'l. Symp. on Combust.* Chicago, IL (2004).

Table 1

Simulation parameters. In all cases: $Da \approx 50$, $\alpha = 0.75$, $\beta = 8.0$, $Pr = 0.75$, $Le = 1.0$, and $\gamma = 1.4$.

Case	2D/3D	Grid	$\kappa_{P,2} l_{11}$	u_0'/s_l	L_i/δ_l	Re_0
Case 0	2D	451^2	0.0^a	15.2	8.9	65.
Case 1	2D	451^2	0.1	15.2	8.9	65.
Case 2	2D	451^2	1.0	15.2	8.9	65.
Case 3	2D	451^2	10.0	15.2	8.9	65.
Case 4	3D	144^3	1.0	37.5	6.0	125.

[a]Baseline case without thermal radiation.

List of Figures

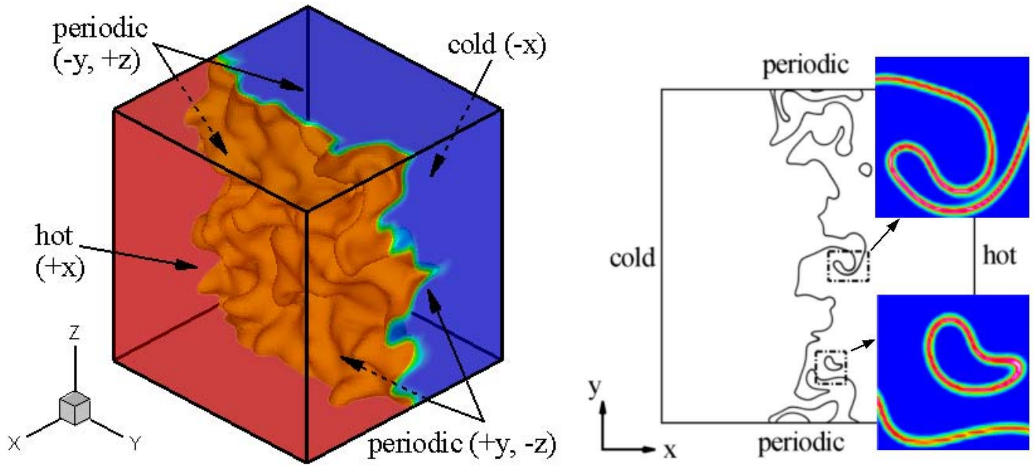

Fig. 1. The computational configuration. Left: Instantaneous temperature isocontours after four eddy-turnover times for Case 4. The $-x$ boundary is a "cold" radiation boundary, and the $+x$ boundary is a "hot" radiation boundary. Right: Instantaneous heat release $Q\dot{w}$ after four eddy-turnover times for Case 1.

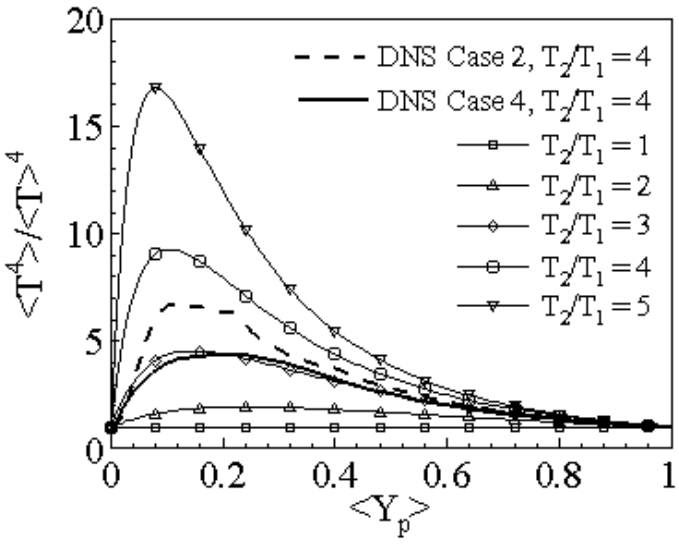

Fig. 2. Temperature self-correlation $\mathcal{R}_{T^4}$, Eq. (5), versus mean progress variable $\langle Y_P \rangle$ for 2D Case 2 (dashed line) and 3D Case 4 (solid line). Also shown are values predicted using a flamesheet approximation [$\mathcal{R}_{T^4\,\mathrm{sheet}}$, Eq. (12)] for several values of T_2/T_1 (lines with symbols).

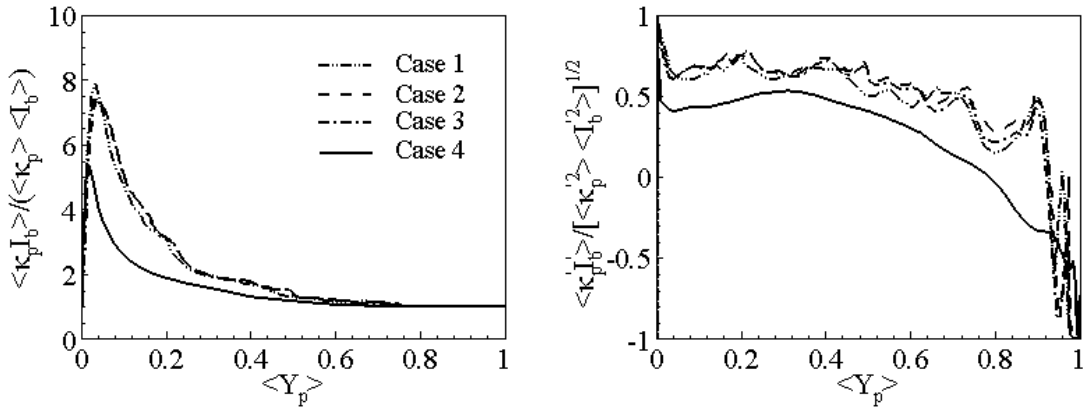

Fig. 3. Absorption coefficient-Planck function correlation factor $\mathcal{R}_{\kappa I_b}$ (left) and correlation coefficient $\rho_{\kappa I_b}$ (right) versus mean progress variable $\langle Y_P \rangle$ for three values of the optical thickness.

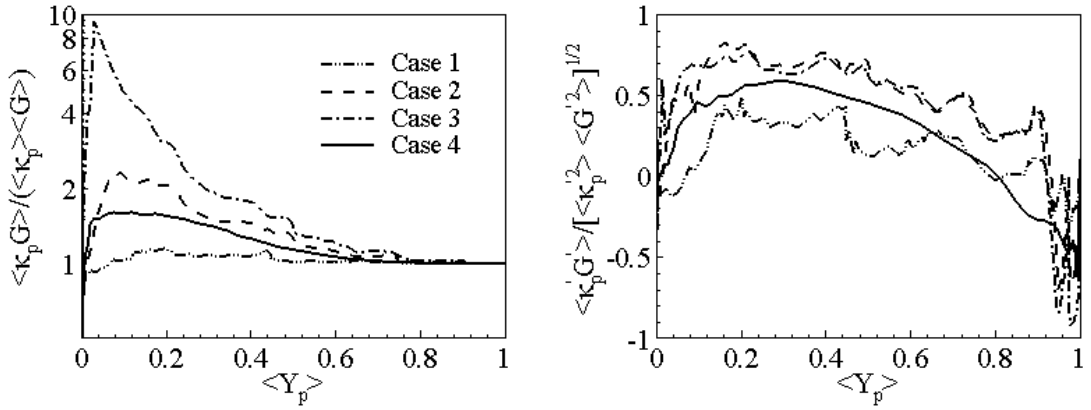

Fig. 4. Absorption coefficient-intensity correlation factor $\mathcal{R}_{\kappa G}$ (left) and correlation coefficient $\rho_{\kappa G}$ (right) versus mean progress variable $\langle Y_P \rangle$ for three values of the optical thickness.